Neurobiology of Aging 66 (2018) 49–58

Contents lists available at ScienceDirect

Neurobiology of Aging

journal homepage: www.elsevier.com/locate/neuaging

Longitudinal and cross-sectional structural magnetic resonance imaging correlates of AV-1451 uptake

Sandhitsu R. Das [a,b,c,d,*], Long Xie [b,e], Laura E.M. Wisse [b,e], Ranjit Ittyerah [b,e], Nicholas J. Tustison [f], Bradford C. Dickerson [g], Paul A. Yushkevich [b,e], David A. Wolk [a,c,d], for the Alzheimer's Disease Neuroimaging Initiative [1]

[a] Department of Neurology, University of Pennsylvania, Philadelphia, PA, USA
[b] Penn Image Computing and Science Laboratory, University of Pennsylvania, Philadelphia, PA, USA
[c] Penn Memory Center, University of Pennsylvania, Philadelphia, PA, USA
[d] Penn Alzheimer's Disease Core Center, University of Pennsylvania, Philadelphia, PA, USA
[e] Department of Radiology, University of Pennsylvania, Philadelphia, PA, USA
[f] Department of Radiology and Medical Imaging, University of Virginia, Charlottesville, VA, USA
[g] Frontotemporal Disorders Unit, Department of Neurology, Massachusetts General Hospital and Harvard Medical School, Boston, MA, USA

ARTICLE INFO

Article history:
Received 11 September 2017
Received in revised form 30 January 2018
Accepted 31 January 2018
Available online 9 February 2018

Keywords:
Alzheimer's disease
Amyloid positive
Amyloid negative
^{18}FAV-1451
Tau
Uptake
PET
Atrophy
Longitudinal
Rate of change
Thickness correlation

ABSTRACT

We examined the relationship between in vivo estimates of tau deposition as measured by ^{18}F-AV-1451 tau positron emission tomography imaging and cross-sectional cortical thickness, as well as rates of antecedent cortical thinning measured from magnetic resonance imaging in individuals with and without evidence of cerebral amyloid in 63 participants from the Alzheimer's Disease Neuroimaging Initiative study, including 32 cognitively normal individuals (mean age 74 years), 27 patients with mild cognitive impairment (mean age 76.8 years), and 4 patients diagnosed with Alzheimer's disease (mean age 80 years). We hypothesized that structural measures would correlate with ^{18}F-AV-1451 in a spatially local manner and that this correlation would be stronger for longitudinal compared to cross-sectional measures of cortical thickness and in those with cerebral amyloid versus those without. Cross-sectional and longitudinal estimates of voxelwise atrophy were made from whole brain maps of cortical thickness and rates of thickness change. In amyloid-β–positive individuals, the correlation of voxelwise atrophy across the whole brain with a summary measure of medial temporal lobe (MTL) ^{18}F-AV-1451 uptake demonstrated strong local correlations in the MTL with longitudinal atrophy that was weaker in cross-sectional analysis. Similar effects were seen in correlations between 31 bilateral cortical regions of interest. In addition, several nonlocal correlations between atrophy and ^{18}F-AV-1451 uptake were observed, including association between MTL atrophy and ^{18}F-AV-1451 uptake in parietal lobe regions of interest such as the precuneus. Amyloid-β–negative individuals only showed weaker correlations in data uncorrected for multiple comparisons. While these data replicate previous reports of associations between ^{18}F-AV-1451 uptake and cross-sectional structural measures, the current results demonstrate a strong relationship with longitudinal measures of atrophy. These data support the notion that in vivo measures of tau pathology are tightly linked to the rate of neurodegenerative change.

1. Introduction

Deposition of paired helical filament tau neurofibrillary tangles (NFTs) along with accumulation of amyloid-β (Aβ) plaques is a hallmark pathology of Alzheimer's disease (AD) (Hyman and Trojanowski, 1997). Ex vivo studies have shown clear associations between NFT burden and antemortem patterns of gray matter atrophy measured by magnetic resonance imaging (MRI) in AD (Whitwell et al., 2008, 2012). Recent advances in molecular imaging have made it possible to quantify regional tau burden in vivo

* Corresponding author at: Department of Neurology, University of Pennsylvania, 3600 Hamilton Walk #602, Philadelphia, PA 19104, USA. Tel.: +1 215 746 7224; fax: 215-573-4060.
E-mail address: sudas@seas.upenn.edu (S.R. Das).

[1] Data used in preparation of this article were obtained from the Alzheimer's Disease Neuroimaging Initiative (ADNI) database (adni.loni.usc.edu). As such, the investigators within the ADNI contributed to the design and implementation of ADNI and/or provided data but did not participate in analysis or writing of this report. A complete listing of ADNI investigators can be found at: http://adni.loni.usc.edu/wp-content/uploads/how_to_apply/ADNI_Acknowledgement_List.pdf.

0197-4580/$ – see front matter © 2018 Elsevier Inc. All rights reserved.
https://doi.org/10.1016/j.neurobiolaging.2018.01.024

(Saint-Aubert et al., 2017). ^{18}F-AV-1451 is a positron emission tomography (PET) tracer that has been used to measure tau deposition due to its selective binding to certain insoluble forms of tau in paired helical filaments (Marquié et al., 2015). ^{18}F-AV-1451 tau tracer uptake has been reported to broadly replicate patterns of NFT deposition based on widely used neuropathological stages (i.e., Braak stages) of AD defined by autopsy studies (Braak and Braak, 1991, 1996)—beginning in medial temporal lobe (MTL), advancing to lateral temporal lobe, inferior frontal, midline and inferior parietal regions, and finally to primary sensorimotor cortices in the latter stages (Cho et al., 2016a; Johnson et al., 2016; Schwarz et al., 2016; Schöll et al., 2016). To the extent that NFT pathology is responsible for downstream neurodegeneration across the disease spectrum and that ^{18}F-AV-1451 binds to AD-related species of tau, structural MRI, an established measure of AD-related neurodegeneration, should be correlated with tracer uptake. Indeed, there are a few reports in which quantitative structural measures have been found to be associated with specific spatial patterns of tau deposition measured using ^{18}F-AV-1451 tau tracer uptake, similar to those observed in pathology studies (Wang et al., 2016; Xia et al., 2017). While there is emerging data with regard to the spatial correlation of ^{18}F-AV-1451 uptake with both local and distant cross-sectional structural measures (Dronse et al., 2017; Golla et al., 2017; Iaccarino et al., 2018; Lockhart et al., 2017; Ossenkoppele et al., 2016; Rafii et al., 2017; Schöll et al., 2016; Sepulcre et al., 2016; Vemuri et al., 2017), the extent of these relationships remains far from clearly delineated. Furthermore, longitudinal atrophy rates, a more direct measure of the dynamic process of neurodegeneration, have not been studied in the context of tau accumulation across the AD continuum, although 1 study reported local and distant correlations of tau burden and retrospective longitudinal atrophy in a cohort consisting of only cognitively normal individuals (LaPoint et al., 2017). Finally, the significance and association of ^{18}F-AV-1451 PET with atrophy in Aβ-negative control subjects is uncertain.

In this study, we aimed to extend work on relationships between ^{18}F-AV-1451 tau tracer uptake and atrophy by investigating longitudinal measures of atrophy. We hypothesized that in a cohort of Aβ-positive individuals that includes both asymptomatic and symptomatic subjects (both mild cognitive impairment [MCI] and AD), the association of local tau deposition in MTL will be stronger with a longitudinal than cross-sectional measure of atrophy, as this would better reflect an active neurodegenerative process specific to tau pathology. If ^{18}F-AV-1451 PET is sensitive to the NFT pathology associated with aging in the absence of cerebral amyloid, so-called primary age-related tauopathy (PART), and this pathology has downstream neurodegenerative effects, we would also expect correlation of ^{18}F-AV-1451 uptake with structural measures in Aβ-negative individuals, but likely circumscribed to early Braak regions.

We studied structural MRI and ^{18}F-AV-1451 PET imaging data in 63 participants from the Alzheimer's Disease Neuroimaging Initiative (ADNI). We correlated a summary measure of ^{18}F-AV-1451 tau tracer uptake in the MTL with cortical thickness–based measures of both cross-sectional and longitudinal atrophies at each voxel in the cortical gray matter. We chose to focus on MTL tracer uptake in a region encompassing perirhinal (including transentorhinal cortex) and entorhinal cortices as these are the earliest regions of NFT deposition, given the significant proportion of individuals who were cognitively normal in this cohort and, thus, likely at early disease stage. More broadly, we conducted a cross-modality pairwise correlation analysis in both cross-sectional and longitudinal data between ^{18}F-AV-1451 tau tracer uptake and atrophy across 31 bilateral regions of interest (ROIs) in the cortex. We performed these analyses separately in Aβ-positive and Aβ-negative groups, as determined by their amyloid PET scans.

2. Materials and methods

2.1. Participants

Data used in the preparation of this article were obtained from the ADNI database. The current study included data from 63 participants. Thirty-two were Aβ-positive, including 13 cognitively normal elderly controls, 15 patients with MCI, and 4 patients diagnosed with AD. Thirty-one were Aβ-negative, including 19 cognitively normal and 12 MCI patients. A summary of participants' demographic characteristics and basic psychometric measures are reported in Table 1. The Aβ-positive and Aβ-negative groups differed in their age, Mini Mental State Examination (MMSE), and Clinical Dementia Rating - Sum of Boxes (CDR-SB) scores.

2.2. Image acquisition

Two T1-weighted structural MRI scans with voxel size 1.0 × 1.0 × 1.2 mm^3 were used. The cross-sectional scan was chosen to be the closest in time to and acquired within 75 days on average of the tau PET scan, and an antecedent MRI was acquired 638 days on average before the cross-sectional scan to measure longitudinal atrophy (see Table 2). Tau PET imaging consisted of a continuous 30-minute brain scan (6 frames of 5-minute duration) 75 minutes following approximately 10 mCi of ^{18}F-AV-1451 injection. Amyloid PET florbetapir protocol used an injection of 10 mCi of tracer and a 20-minute brain scan (4 frames of 5-minute duration) after a 50-minute uptake phase. The florbetapir scan acquired closest in time to the ^{18}F-AV-1451 scan was analyzed (see Table 2). Note that 2 scans in amyloid-positive individuals were obtained >2 years before the ^{18}F-AV-1451 PET. As one would not expect a positive scan to become negative over time, we included these individuals despite this delay. PET images were downloaded from the ADNI data archive in the most fully preprocessed format with the image description "Coreg, Avg, Std Img and Vox Siz, Uniform Resolution."

Table 1
Demographic information for participants

Amyloid/clinical status (N)	Age (y)	Education (y)	MMSE	CDR-SB	CDR-global
Positive/all (32)	78.7 ± 5.9[a]	16.3 ± 2.4	27.2 ± 3.4[a]	1.55 ± 2.38[a]	0.34 ± 0.36
Positive/CTL (13)	77.4 ± 5.1	16.4 ± 1.4	28.5 ± 1.5	0.05 ± 0.16	0.00 ± 0.00
Positive/MCI (15)	79.3 ± 6.5	16.1 ± 3.2	27.8 ± 2.2	1.17 ± 1.08	0.40 ± 0.21
Positive/AD (4)	81.0 ± 6.2	16.5 ± 1.9	21.0 ± 5.2	6.75 ± 1.71	1.00 ± 0.00
Negative/all (31)	72.4 ± 6.0	16.6 ± 2.4	29.0 ± 1.5	0.52 ± 0.76	0.19 ± 0.25
Negative/CTL (19)	71.7 ± 5.2	16.0 ± 2.6	29.4 ± 0.8	0.21 ± 0.40	0.09 ± 0.20
Negative/MCI (12)	73.7 ± 7.3	17.6 ± 1.8	28.5 ± 2.2	0.96 ± 0.94	0.33 ± 0.25

Key: AD, Alzheimer's disease; CTL, control; MCI, mild cognitive impairment.
[a] Indicates significant difference between amyloid-positive and -negative groups.

Table 2
Time difference in days between scans indicated as mean ± standard (max)

Amyloid status (N)	T − S1	T − S2	T − A
Positive (32)	756 ± 205[a] (1115)	83 ± 109 (372)	198 ± 252 (1090)
Negative (31)	667 ± 216 (1117)	65 ± 126 (478)	190 ± 191 (483)

Key: A, amyloid PET; MRI, magnetic resonance imaging; PET, positron emission tomography; S1, retrospective MRI; S2, cross-sectional MRI; T, tau PET.
[a] Indicates significant difference between groups at $p < 0.05$.

2.3. Image processing

The preprocessed PET images were aligned with the anatomical MRI via rigid body registration using the Advanced Normalization Tools (ANTs) normalization software (Avants et al., 2008, 2014) with a mutual information metric. Each anatomical MRI was segmented into cortical, subcortical, and cerebellar ROIs using a multiatlas segmentation method (Wang et al., 2013). The parcellation scheme is described in (Landman and Warfield, 2012) (https://www.amazon.com/MICCAI-2012-Workshop-Multi-Atlas-Labeling/dp/1479126187). Mean tracer uptake in the cerebellar gray matter (^{18}F-AV-1451) or cerebellar gray and white matters (florbetapir) was computed and used as reference to generate a standardized uptake value ratio (SUVR) map for the entire brain. A composite ROI consisting of middle frontal, anterior cingulate, posterior cingulate, inferior parietal, precuneus, supra marginal, middle temporal, and superior temporal cortices was used to compute a global SUVR for florbetapir. A threshold of SUVR $\geq$ 1.11 (Landau et al., 2013) was then used to determine Aβ status.

Cortical thickness was estimated using the DiReCT method (Das et al., 2009) implemented in the ANTs longitudinal measurement pipeline (Tustison et al., 2014, 2017). This method uses diffeomorphic mapping between the white matter-gray matter boundary and gray matter-cerebrospinal fluid boundary derived from tissue segmentation to estimate cortical thickness and produces a volumetric map of local thickness at every voxel in the cortex. An evaluation of DiReCT in relation to other cortical thickness measurement methods can be found in the studies by Klein et al., 2009 and Tustison et al., 2014. Longitudinal estimation used an unbiased method that treats each scan in similar fashion such that the measurements at each time point do not depend on their temporal ordering (Avants et al., 2010). The resulting maps of thickness and thickness change were mapped to an unbiased population template (Avants and Gee, 2004) for voxelwise analysis. A summary measure of MTL ^{18}F-AV-1451 tau tracer uptake was computed over a combined ROI of entorhinal cortex and BA35 and BA36 regions of perirhinal cortex using a multiatlas segmentation algorithm specific for these regions (Xie et al., 2016; Yushkevich et al., 2015).

The entire brain for both structural scans in each subject was parcellated into 31 bilateral ROIs based on a previously published volumetric version of the FreeSurfer Desikan-Killiany-Tourville atlas (Klein and Tourville, 2012), using a multiatlas segmentation method (Wang et al., 2013). These ROIs were used to generate mean cortical thickness estimates averaged across bilateral regions. Average longitudinal thickness change for each ROI was entered in analysis as an annualized rate of change in mm. Similarly, mean SUVR for ^{18}F-AV-1451 uptake was also calculated for each bilateral ROI.

2.4. Statistical analysis

Partial correlation was used for assessing relationships between the 2 imaging measurements in Aβ-positive and Aβ-negative groups separately. Covariates used were as follows: (1) age and (2) time between cross-sectional MRI and tau PET (cross-sectional analysis) or time between antecedent MRI and tau PET (longitudinal analysis). Note that use of gender as a covariate did not appreciably influence results of these analyses. We performed voxelwise correlation of a summary measure of average ^{18}F-AV-1451 tau tracer uptake in bilateral MTL with cross-sectional cortical thickness as well as with rate of cortical thickness change in the preceding time period. Multiple comparisons correction was done using the threshold-free cluster enhancement method (Smith and Nichols, 2009). We then performed a cross-modality ROI-based correlation analysis across the entire brain where ^{18}F-AV-1451 tau tracer uptake was correlated with both cross-sectional and longitudinal measures of cortical thickness between each pair of the 31 ROIs. Permutation-based p-values were computed and subsequently corrected for multiple comparisons using false discovery rate (Yekutieli and Benjamini, 1999). As a supplementary analysis, we directly compared the cross-sectional and longitudinal correlations using the correlation comparison test described by Diehl and Arbinger, 1992.

3. Results

3.1. Spatial distribution of ^{18}F-AV-1451 tau tracer uptake

Fig. 1 top panel shows patterns of ^{18}F-AV-1451 uptake by mean SUVR within each group of participants, as well as a statistical map of significantly greater tracer uptake in Aβ-positive individuals. These maps show that spatial extent of significant tau accumulation is limited and is primarily confined to the temporal lobe in the Aβ-positive individuals. In those without cerebral amyloid, it is even more restricted largely just to MTL. However, even within the MTL, uptake is significantly higher in the Aβ-positive individuals. Fig. 1 bottom panel shows statistical maps of group difference in cross-sectional and longitudinal measures of atrophy. Group effects are much weaker for atrophy than for tracer uptake. No voxels survived multiple comparisons correction. The effects in data uncorrected for multiple comparisons are more localized, with the longitudinal effects being generally stronger, especially in medial regions such as the MTL.

3.2. Voxelwise correlations

Figs. 2 and 3 show patterns of correlation of voxelwise cortical thickness and longitudinal rate of thickness change with a summary measure of MTL ^{18}F-AV-1451 tau tracer uptake. Longitudinal rate of thickness change in the MTL, particularly in the entorhinal and perirhinal cortices, had a strong and statistically significant relationship with ^{18}F-AV-1451 uptake bilaterally in Aβ-positive individuals. Cross-sectional thickness measurements showed a similar pattern in this group, but fewer voxels survived correction for multiple comparisons. More diffuse effects were observed only in data uncorrected for multiple comparisons (Fig. 2B,D), which also show an extensive pattern of remote correlations of thickness with MTL ^{18}F-AV-1451 uptake in both the cross-sectional and longitudinal analysis, with the former showing more widespread effects with the more liberal threshold. Scatterplots of some significant clusters are shown as insets. As can be observed, 1 participant in the Aβ-positive group who had a diagnosis of probable AD had very high longitudinal atrophy rates in the MTL as well as the highest ^{18}F-AV-1451 uptake in this region. We visually checked for imaging and processing-related artifacts in the data and did not find any anomalies. Excluding this data point would still maintain a strong and significant correlation for this cluster ($r = -0.76$, $p < 10e^{-7}$ with and $r = -0.67$, $p < 10e^{-5}$ without). In Aβ-negative individuals (Fig. 3), while there are no significant effects that survived multiple comparisons correction, some regions showed correlation in the uncorrected data, particularly in the precuneus in the cross-sectional data.

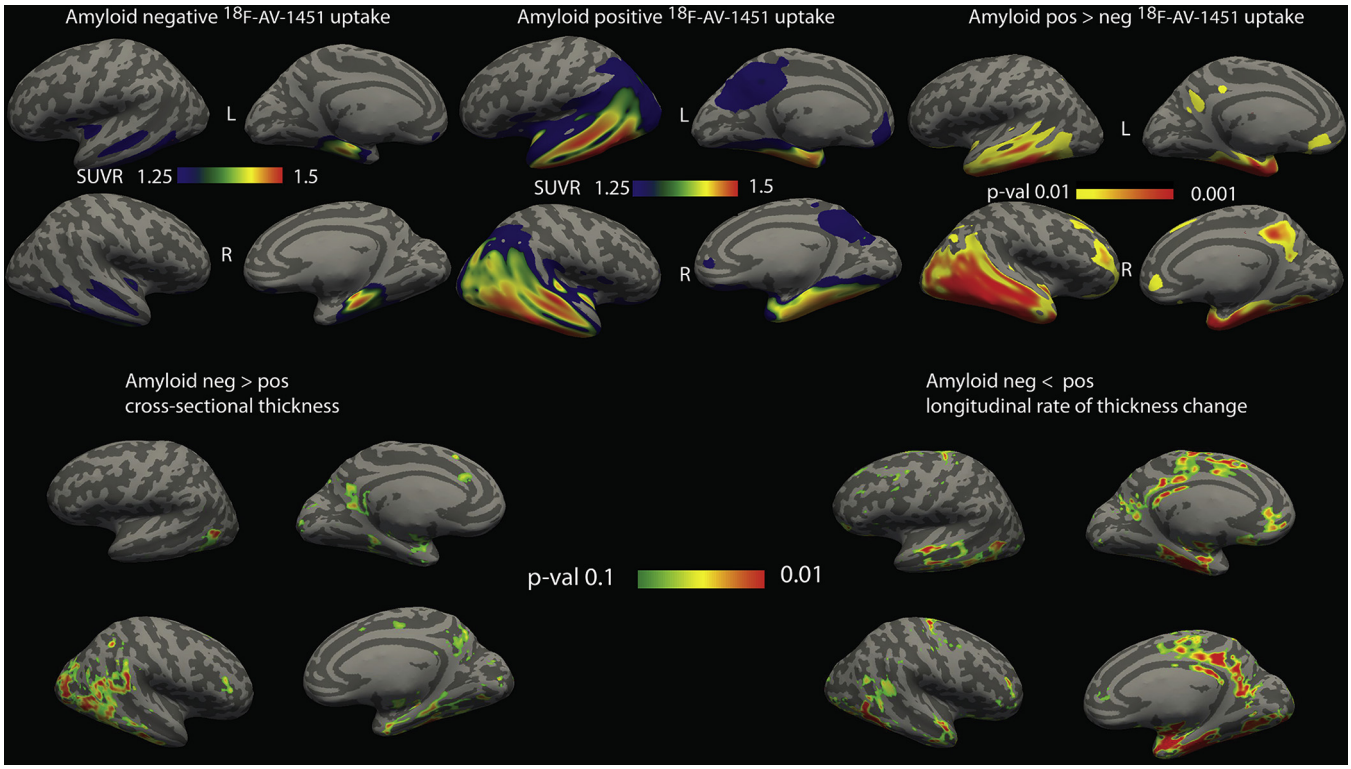

Fig. 1. Top: mean SUVR of ^{18}F-AV-1451 uptake in amyloid-negative (left) and amyloid-positive (middle) individuals. Right panel shows areas of significantly greater tracer uptake in amyloid-positive group ($p < 0.01$ FWER). Bottom: areas of significantly greater thickness (left) and lower rate of thickness change (right) in amyloid-negative individuals. Maps are shown at an uncorrected threshold of $p < 0.1$ for visualizing trends in the data. Effects were not statistically significant after correction for multiple comparisons. Abbreviations: SUVR, standardized uptake value ratio.

3.3. ROI-based correlations

Figs. 4 and 5 summarize cross-modality relationships between atrophy and ^{18}F-AV-1451 uptake across pairs of ROIs using a matrix representation that captures both local (diagonal elements) and distant (off-diagonal elements) correlations between tau pathology and cross-sectional/longitudinal measures of structural atrophy.

Similar to the voxelwise analysis, longitudinal rates of MTL cortical thinning (left panel) and cross-sectional measures of thickness (right panel) were significantly correlated with ^{18}F-AV-1451 uptake in MTL ROIs in Aβ-positive individuals (Fig. 4). In addition to local MTL effects, lateral temporal lobe ROIs showed significant local cross-modality correlations in Aβ-positive individuals. Moreover, both cross-sectional and longitudinal measures of atrophy in multiple temporal ROIs correlated with ^{18}F-AV-1451 uptake in a wide swath of brain regions in the lobes outside of occipital, including parietal lobe regions such as inferior parietal, precuneus and posterior cingulate regions, and several ROIs in the frontal lobe, including orbitofrontal and anterior cingulate cortices. These nonlocal correlations of ^{18}F-AV-1451 uptake the in parietal and frontal lobes with temporal lobe atrophy were stronger and more restricted to MTL ROIs, such as the entorhinal cortex, in the longitudinal data. Alternatively, the cross-sectional effects were more diffuse across the temporal lobe and strongest in the inferior temporal and fusiform ROIs. While there were modest local correlations outside of the temporal lobe, longitudinal data also showed strong correlation of atrophy rates in some frontal lobe regions such as the orbitofrontal cortex with ^{18}F-AV-1451 uptake in largely the same set of regions that had strong correlations with temporal lobe atrophy.

Supplementary analysis showing direct comparison of the ROI-based cross-sectional and longitudinal correlations is presented in Supplementary Figure S1. Some MTL regions such as the entorhinal and parahippocampal cortices and orbitofrontal cortex showed stronger correlations in the longitudinal data, whereas other areas showed the opposite trend (fusiform and insular cortices). However, none of these effects reached statistical significance when corrected for multiple comparisons.

As noted previously, 1 participant in the Aβ-positive group had very high atrophy rates in the MTL and the highest ^{18}F-AV-1451 uptake in some temporal lobe regions (see scatter plot in Fig. 2). Permutation testing for the ROI analysis was done to account for such outliers and, additionally, the results were qualitatively similar with weaker effects in the correlation of 18F-AV-1451 uptake in frontal ROIs with temporal atrophy when this participant was excluded from the analysis. Excluding the time difference between MRI and PET scans as a covariate also did not notably alter the results.

We did not find any significant correlation effects after multiple comparisons correction in the Aβ-negative individuals (Fig. 5). However, data uncorrected for multiple comparisons showed a significant correlation of precuneus atrophy with ^{18}F-AV-1451 uptake in a number of ROIs.

4. Discussion

4.1. Local MTL effects in Aβ-positive individuals

We found that a summary measure of MTL ^{18}F-AV-1451 uptake in Aβ-positive individuals was most significantly associated with longitudinal cortical thinning, and this effect was restricted to the

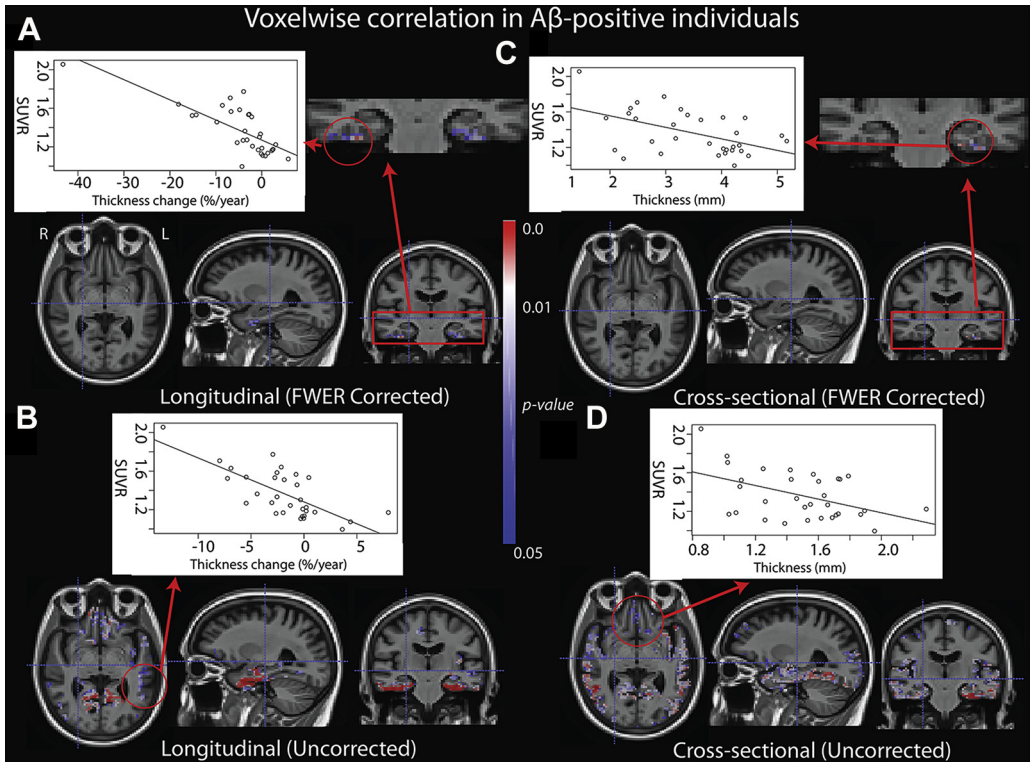

Fig. 2. Significant clusters of partial correlation between MTL cortex tau uptake and atrophy measured as rate of thickness change (A and B) and thickness (C and D) across the brain, with age and time between MRI and PET as nuisance covariates, in Aβ-positive individuals. Panels A and C and panels B and D show *p*-values that have been corrected for multiple comparisons and uncorrected, respectively. Insets in panels A and C show coronal view of MTL and scatterplots of MTL tau versus atrophy in the largest significant cluster in the MTL, indicated by red circles. Similar scatterplots are shown in the panels B and D for significant clusters outside of the MTL in the uncorrected data. Abbreviation: Aβ, amyloid beta; MRI, magnetic resonance imaging; MTL, medial temporal lobe; PET, positron emission tomography. (For interpretation of the references to color in this figure legend, the reader is referred to the Web version of this article.)

MTL in Family-wise Error Rate (FWER)-corrected analysis. This finding supports the significance of tau accumulation measured in vivo by ^{18}F-AV-1451 uptake as a marker of disease burden: greater tau burden is associated with an increased rate of neurodegeneration in the preceding years. In other words, those with higher tracer uptake in the MTL would be expected to have

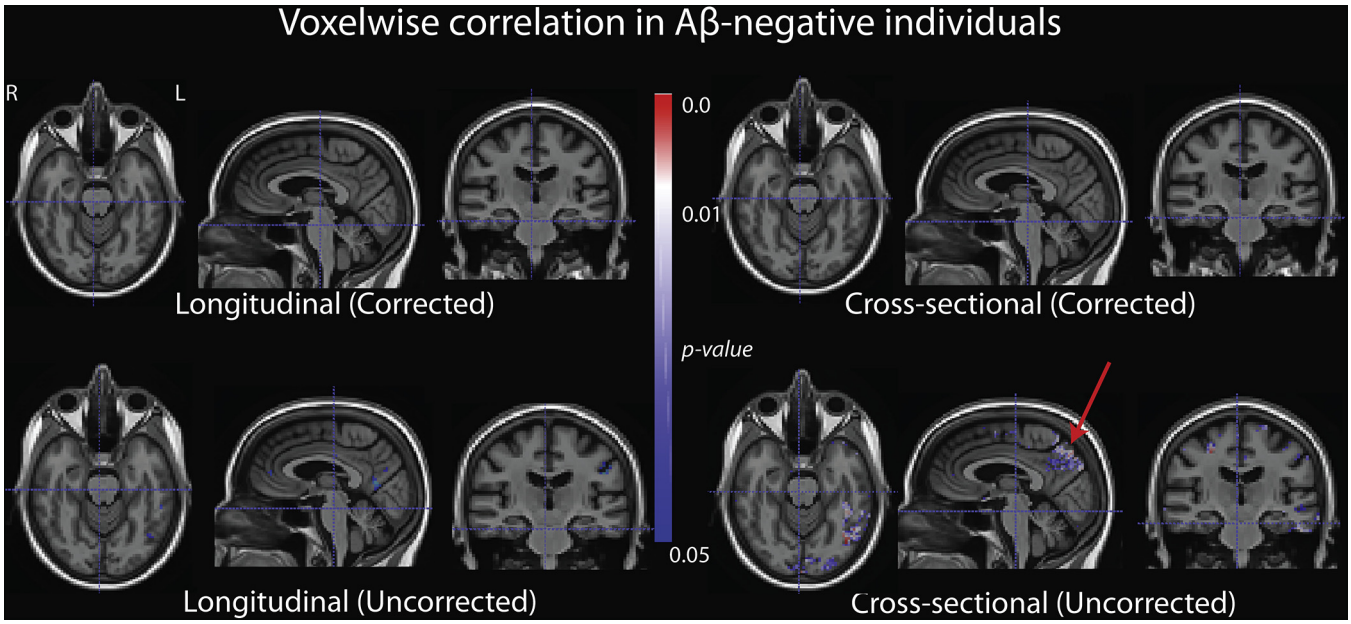

Fig. 3. Significant clusters of partial correlation between MTL cortex tau uptake and atrophy measured as rate of thickness change (left) and thickness (right) across the brain, with age and time between MRI and PET as nuisance covariates, in Aβ-negative individuals. Top and bottom rows show *p*-values that have been corrected for multiple comparisons and uncorrected respectively. Arrow shows an area of effect in the precuneus. Abbreviations: Aβ, amyloid beta; MRI, magnetic resonance imaging; MTL, medial temporal lobe; PET, positron emission tomography.

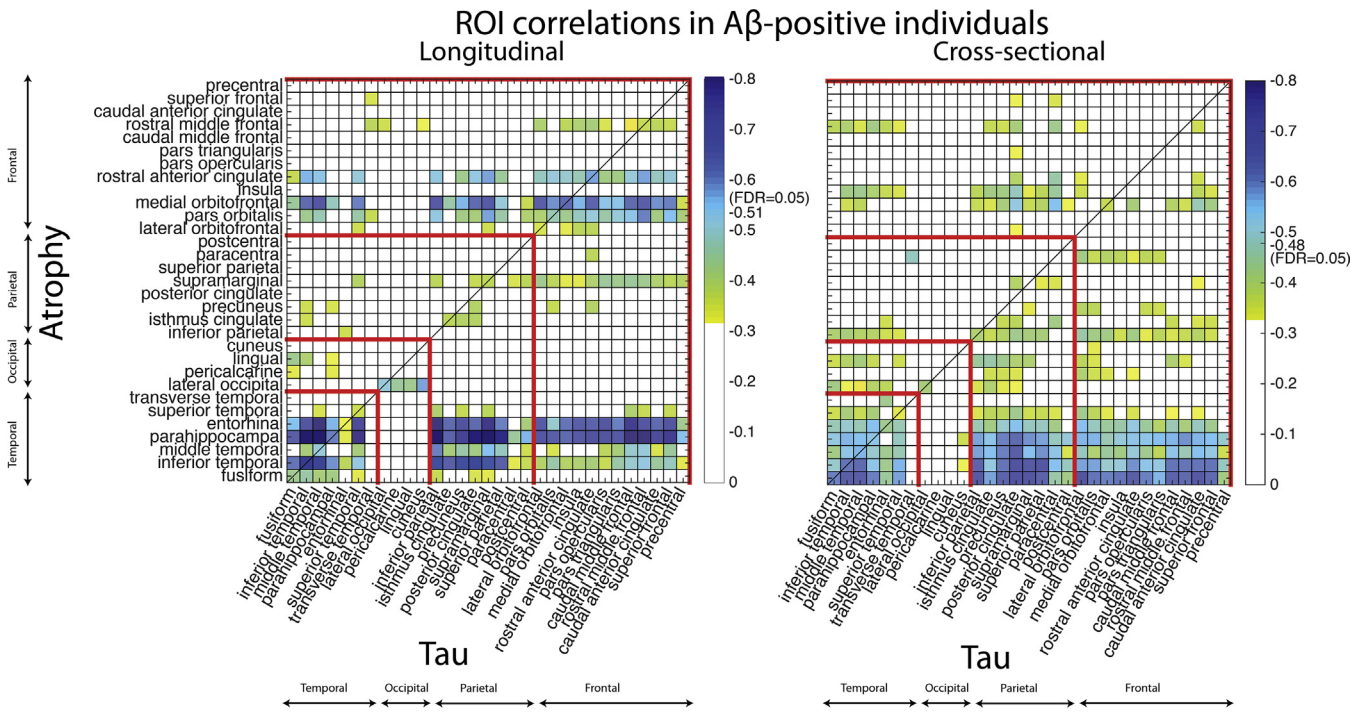

Fig. 4. Partial correlation of ^{18}F-AV-1451 tau tracer uptake and atrophy as measured by rate of thickness change (left) or thickness (right) in 31 ROIs, with age and time between MRI and PET as covariates, in Aβ-positive participants. Columns are sorted with most average ^{18}F-AV-1451 tau tracer uptake on the left and to least on the right. ROIs within a lobe are similarly sorted. Columns and rows represent tau and atrophy, respectively, such that a given row shows correlation between atrophy in an ROI with tau in all other ROIs, and a given column shows correlation between tau in an ROI with atrophy in all other ROIs. Diagonal values represent local correlation of the 2 measures within the same ROI. Nonempty cells denote significant correlation at permutation-based $p < 0.05$ uncorrected. FDR thresholds of $p < 0.05$ correcting for multiple comparisons are indicated in the color bar. Solid blue cells had strongest effect at FDR-corrected $p < 0.01$. Red lines indicate lobes. Abbreviation: Aβ, amyloid beta; FDR, false discovery rate; MRI, magnetic resonance imaging; PET, positron emission tomography; ROI, region of interest. (For interpretation of the references to color in this figure legend, the reader is referred to the Web version of this article.)

experienced more significant neuronal injury commensurate with this greater burden.

The local correlational effect within MTL in the cross-sectional analysis was less robust in the MTL and fewer voxels were significant using the FWER-corrected statistical threshold. However, when pairwise correlations in the ROI analysis were directly compared (Supplementary Figure S1), although some MTL effects were stronger in longitudinal data, the differences were not statistically significant after multiple comparisons correction. Nonetheless, the finding that longitudinal structural measures appear to be more tightly linked with a measure of NFT burden in MTL than cross-sectional structural measures is intuitive. One would expect that a longitudinal measure would reflect the active neurodegeneration in a region over the restricted temporal window of the imaging data acquisitions, which should reflect temporally proximate local pathologies, such as NFT. Alternatively, cross-sectional cortical thickness reflects the sum total of factors influencing the measure of brain structure in that region across the lifespan. These include developmental differences, as well as alterations in neuronal or synaptic density associated with other processes, such as normal aging or cerebrovascular disease, that likely occur over a different timescale than neurodegeneration due to NFTs. Thus, assuming similar measurement accuracy, a longitudinal measure may more accurately reflect the specific neurodegeneration associated with local tau accumulation.

4.2. Relationship between MTL tau tracer uptake and atrophy outside of MTL in Aβ-positive individuals

While the local relationship between MTL tau tracer uptake and atrophy measures is intuitive, it is worth noting that when using a more liberal threshold, there was more spatially widespread association with atrophy in Aβ-positive individuals, particularly in the orbitofrontal region in the longitudinal data and lateral temporal regions in the cross-sectional data (Fig. 2). Strong distant correlation between tau in the temporal lobe and cross-sectional cortical thinning in the orbitofrontal cortex was also reported by Sepulcre et al. (Sepulcre et al., 2016). Furthermore, LaPoint et al. examined retrospective longitudinal atrophy as here and similarly reported local and remote correlations between ^{18}F-AV-1451 uptake in inferior temporal lobe; however, their study was limited to cognitively normal adults and did not dichotomize groups based on amyloid status (LaPoint et al., 2017). The distant effects in ours and these prior studies are likely due in part to the fact that MTL and/or inferior temporal tau tracer uptake, reflecting early NFT pathology, may also serve as a summary measure more broadly for disease progression. Indeed, other work has suggested that ^{18}F-AV-1451 uptake in this region does not plateau across the AD continuum through at least mild AD (Tosun et al., 2017). As such, it is possible that MTL tau serves as a surrogate for local tau burden in these connected regions, which may then locally drive neurodegeneration. In fact, in the ROI analysis (Fig. 4) several, but not all, of the ROIs, where atrophy is correlated with MTL or other temporal region ^{18}F-AV-1451 uptake, also had significant correlation with local uptake (i.e., significant correlation along the diagonal), particularly in the longitudinal data.

4.3. Lack of local effects outside of MTL in Aβ-positive individuals

While as noted previously, there were some local effects observed, such as in orbitofrontal and anterior cingulate regions, particularly in the longitudinal data in Aβ-positive individuals

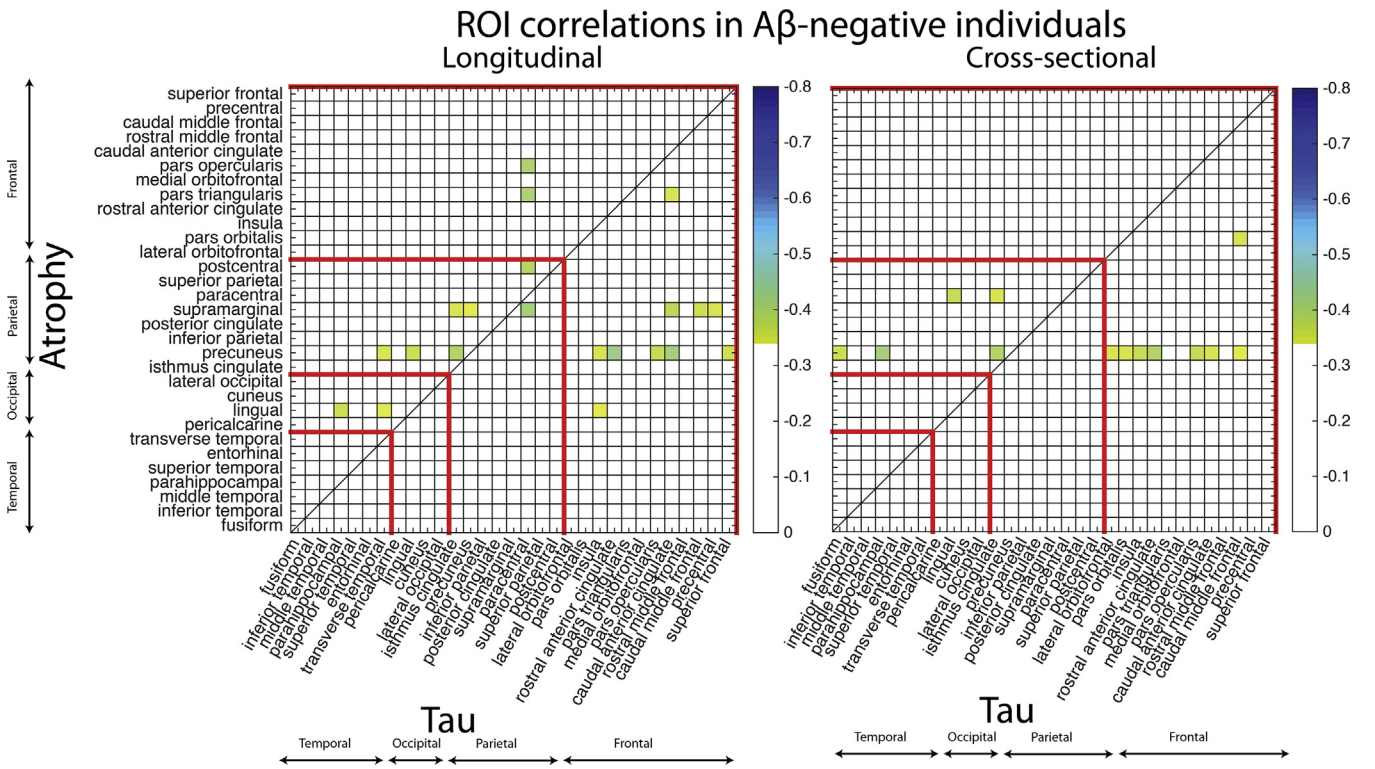

Fig. 5. Partial correlation of ^{18}F-AV-1451 tau tracer uptake and atrophy as measured by rate of thickness change (left) or thickness (right) in 31 ROIs, with age and time between MRI and PET as covariates, in Aβ-negative participants. Red lines indicate lobes, which are presented in the same order as in Fig. 4. Within each lobe, columns are sorted with most average ^{18}F-AV-1451 tau tracer uptake on the left and to least on the right. Rows are sorted in the same order. Columns and rows represent tau and atrophy, respectively, such that a given row shows correlation between atrophy in an ROI with tau in all other ROIs, and a given column shows correlation between tau in an ROI with atrophy in all other ROIs. Diagonal values represent local correlation of the 2 measures within the same ROI. Nonempty cells denote significant correlation at permutation-based $p < 0.05$ uncorrected for multiple comparisons. No correlations survived FDR correction for multiple comparisons. Abbreviation: Aβ, amyloid beta; FDR, false discovery rate; MRI, magnetic resonance imaging; PET, positron emission tomography; ROI, region of interest. (For interpretation of the references to color in this figure legend, the reader is referred to the Web version of this article.)

(Fig. 4, left), many extratemporal regions typically associated with AD-related atrophy did not display local (or distant) correlation with tracer uptake. The fact that there were not always strong local correlations of atrophy and ^{18}F-AV-1451 uptake in regions outside of the temporal lobe might be explained simply by the lack of significant tau pathology outside of this region in this cohort, as reflected by relatively low ^{18}F-AV-1451 uptake (Fig. 1). While significant ^{18}F-AV-1451 tau tracer uptake in parietal ROIs have been reported in several studies in Aβ-positive individuals (Schöll et al., 2016; Xia et al., 2017), with concomitant thinning in these regions observed (Xia et al., 2017), this subset of the ADNI cohort has revealed more restricted uptake to temporal regions (also see Maas et al. [Maass et al., 2017]). Finally, in the case of the longitudinal data, limited local correlations might also be a reflection of a potential nonlinear trajectory of cortical thinning, which may depend on baseline thickness.

While not displaying widespread local correlation in nontemporal regions, we did observe significant correlation of MTL inferomedial temporal cortical atrophy with ^{18}F-AV-1451 uptake in a wide swath of ROIs outside of the temporal lobe (Fig. 4 bottom rows), in a number of isocortical regions, particularly parietal and frontal. This suggests that even at low levels of tau, accumulation of tau into extratemporal regions may be a surrogate for disease progression, reflecting spread of tau pathology outside the temporal lobe. To the extent that MTL atrophy reflects disease stage, we might, therefore, expect to observe a relationship with extratemporal tau. Alternatively, these more distant relationships of ^{18}F-AV-1451 uptake with temporal regions may be mediated by propagation of tau pathology across connected regions, providing support for the synaptic transmission hypothesis (Frost et al., 2009; Lewis and Dickson, 2016). Some ROIs showing these effects indeed constitute nodes of the same functional network (e.g., MTL and posterior cingulate are considered parts of the default mode network, and orbitofrontal cortex is part of an anterior temporal lobe network [Das et al., 2015]).

4.4. Lack of effects in Aβ-negative individuals

We did not find strong correlations between ^{18}F-AV-1451 and cross-sectional or longitudinal measures in Aβ-negative individuals. The only significant correlation of MTL ^{18}F-AV-1451 uptake with atrophy observed in the Aβ-negative individuals was in the precuneus region (Fig. 3), but only in data uncorrected for multiple comparisons. While this effect was weak, it is interesting to note that ^{18}F-AV-1451 uptake in multiple other ROIs also appeared to correlate with precuneus atrophy (Fig. 5). Interestingly, in this group, cross-sectional data appeared to have a stronger effect, which may be a result of any association between ^{18}F-AV-1451 and atrophy occurring on a slower timescale in this group than in Aβ-positive individuals and, thus, not well captured within the 2-year timeframe of the longitudinal analysis.

The Aβ-negative group contained a mixture of cognitively normal adults (n = 19) and patients with MCI (n = 12). While other studies, such as the study by Sepulcre et al., 2016, reported significant local and remote associations between gray matter atrophy and ^{18}F-AV-1451 uptake in a cognitively normal elderly cohort,

these studies have not examined such effects in Aβ-negative individuals alone. As seen in Fig. 1, ^{18}F-AV-1451 uptake in this group in the ADNI cohort is generally very low and much lower throughout the temporal lobe compared to the Aβ-positive individuals as revealed by the group comparison. For example, the MTL summary measure of tracer uptake in the Aβ-negative group was lower on average with a much smaller range (SUVR mean 1.15, standard deviation = 0.08, range 0.97–1.36) than the Aβ-positive group (mean 1.37, standafrd = 0.25, range 1.0–2.06). Compared to the Aβ-positive group, they were also relatively younger and had a higher proportion of cognitively normal participants. These might further influence correlation of tracer uptake with atrophy. Given this low tau burden in the MTL, as well as the fact that at these low levels effects of "noise" in this region, for example, from off-target choroid plexus binding (Lowe et al., 2016; Pontecorvo et al., 2017) may be more prominent, other factors may be more likely to drive differences in cortical thickness and rate of atrophy in these individuals than MTL ^{18}F-AV-1451 uptake. The current result is consistent with another recent report from Mormino et al. (Mormino et al., 2016) in which Aβ-negative individuals, with versus without evidence of neurodegeneration, measured by hippocampal volume or cortical glucose metabolism, did not differ in ^{18}F-AV-1451 uptake. The authors suggested that PART (Crary et al., 2014), a common feature of early aging defined by the presence of NFTs of Braak stage IV or less (usually stages I–III) in the absence of amyloid, was not the driver of the neurodegeneration observed in that cohort.

The current finding also could be interpreted as supporting the notion that the presence of PART is not tightly linked to atrophy, including within the MTL. However, a recent study did find correlation of antemortem anterior hippocampal atrophy and Braak NFT stage in PART individuals (Josephs et al., 2017). While we did not measure hippocampal volume, that cohort was considerably older (mean age of 90 years at death) than the current amyloid-negative group, which may have influenced our finding evidence of similar MTL atrophy, particularly given the link between PART severity and age. An alternative hypothesis is that the ^{18}F-AV-1451 ligand may not bind avidly to the specific conformation of tau associated with PART. Indeed, recent autoradiography findings suggest that ^{18}F-AV-1451 binding to the generally more immature tangles of PART was relatively weak (Lowe et al., 2016).

4.5. ^{18}F-AV-1451 as a marker linking tau pathology to AD-related neurodegeneration

Prior studies have shown that ^{18}F-AV-1451 tau tracer uptake patterns reflect clinical phenotypes and associated neuroanatomical variability in AD (Cho et al., 2016a; Ossenkoppele et al., 2016; Schwarz et al., 2016). The relationship between ^{18}F-AV-1451 tau tracer uptake and structural atrophy has also been reported in a number of cross-sectional analyses (Sepulcre et al., 2016; Xia et al., 2017). The strong association between ^{18}F-AV-1451 uptake and longitudinal atrophy rates in an Aβ-positive cohort presented here, particularly within the MTL, lends support to the notion that the ^{18}F-AV-1451 tracer links AD-related pathology to the accelerated neurodegeneration associated with NFT pathology. Not surprisingly, given this relationship, increased ^{18}F-AV-1451 uptake is associated with increased cognitive impairment in Aβ-positive individuals (Cho et al., 2016b; Johnson et al., 2016; Pontecorvo et al., 2017). Consonant with the structural MRI findings here, Schöll et al., 2016 found that ^{18}F-AV-1451 uptake was correlated with both cross-sectional and antecedent longitudinal cognitive measures, particularly episodic memory. Importantly, the data here support the value of MRI-based atrophy measurements, along with cognition, for tracking the effects of NFT pathology in AD.

4.6. Limitations and future work

One limitation of the current study is that longitudinal atrophy was measured during a time period before the ^{18}F-AV-1451 scan. Therefore, a temporal order of tau deposition and neurodegeneration resulting from it cannot be established based on these data. Nonetheless, the strong correlation between the antecedent atrophy rate and ^{18}F-AV-1451 uptake indicates a tight coupling of NFT pathology with the neurodegenerative process. Continued collection of follow-up structural imaging data in ADNI will allow us to look at prospective neurodegenerative changes. Furthermore, a direct comparison of longitudinal measures from both modalities will greatly enhance our understanding of their temporal relationship. Another limitation is the modest sample size, particularly to more definitively determine whether there is any relationship in amyloid-negative individuals between structure and ^{18}F-AV-1451. Such data will be forthcoming from ADNI, as well as other cohorts, over the next several years.

5. Conclusion

We examined association of ^{18}F-AV-1451 tau tracer uptake with cross-sectional as well as longitudinal measures of atrophy based on cortical thickness in separate groups of Aβ-positive and Aβ-negative subjects. The data support a relationship between ^{18}F-AV-1451 tau tracer uptake and evidence of neurodegeneration reflected in structural MRI. The somewhat stronger local linkage with longitudinal estimates in the MTL supports the coupling of tau burden with active, local neurodegeneration that is perhaps more specifically captured by a longitudinal rather than cross-sectional measure due to the other confounding modulators of the latter. The data support the utility and potential parallel information provided by longitudinal structural MRI and ^{18}F-AV-1451 tau PET imaging for tracking AD-related neurodegeneration.

Disclosure statement

BCD receives grant support from Merck (DSMB), Biogen, Lilly, Novartis. DAW receives consulting fees from Merck, Janssen, and Lilly and grant support from Merck, Biogen, and Lilly.

Acknowledgements

Data collection and sharing for this project was funded by the Alzheimer's Disease Neuroimaging Initiative (ADNI) (National Institutes of Health Grant U01 AG024904), and DOD ADNI (Department of Defense award number W81XWH-12-2-0012). ADNI is funded by the National Institute on Aging, the National Institute of Biomedical Imaging and Bioengineering, and through generous contributions from the following: AbbVie, Alzheimer's Association; Alzheimer's Drug Discovery Foundation; Araclon Biotech; BioClinica, Inc; Biogen; Bristol-Myers Squibb Company; CereSpir, Inc; Cogstate; Eisai Inc; Elan Pharmaceuticals, Inc; Eli Lilly and Company; Euroimmun; F. Hoffmann-La Roche Ltd and its affiliated company Genentech, Inc; Fujirebio; GE Healthcare; IXICO Ltd; Janssen Alzheimer Immunotherapy Research & Development, LLC.; Johnson & Johnson Pharmaceutical Research & Development LLC.; Lumosity; Lundbeck; Merck & Co, Inc; Meso Scale Diagnostics, LLC.; NeuroRx Research; Neurotrack Technologies; Novartis Pharmaceuticals Corporation; Pfizer Inc; Piramal Imaging; Servier; Takeda Pharmaceutical Company; and Transition Therapeutics. The Canadian Institutes of Health Research is providing funds to support ADNI clinical sites in Canada. Private sector contributions are facilitated by the Foundation for the National Institutes of Health (www.fnih.org). The grantee organization is the Northern California

Institute for Research and Education, and the study is coordinated by the Alzheimer's Therapeutic Research Institute at the University of Southern California. ADNI data are disseminated by the Laboratory for Neuro Imaging at the University of Southern California.

This work was also supported by National Institutes of Health grant numbers R01 DC014296, R21 AG051987, R01 AG037376, R01 AG056014, R01 EB017255, R03 EB016923, and R01 AG055005 and the donors of Alzheimer's Disease Research, a program of the BrightFocus Foundation (LEMW).

Appendix A. Supplementary data

Supplementary data associated with this article can be found, in the online version, at https://doi.org/10.1016/j.neurobiolaging.2018.01.024.

References

Avants, B., Gee, J.C., 2004. Geodesic estimation for large deformation anatomical shape averaging and interpolation. Neuroimage 23 Suppl 1, S139–S150.

Avants, B., Cook, P.A., McMillan, C., Grossman, M., Tustison, N.J., Zheng, Y., Gee, J.C., 2010. Sparse unbiased analysis of anatomical variance in longitudinal imaging. Med. Image Comput. Comput. Assist. Interv. 13 (Pt 1), 324–331.

Avants, B.B., Epstein, C.L., Grossman, M., Gee, J.C., 2008. Symmetric diffeomorphic image registration with cross-correlation: evaluating automated labeling of elderly and neurodegenerative brain. Med. image Anal. 12, 26–41.

Avants, B.B., Tustison, N.J., Stauffer, M., Song, G., Wu, B., Gee, J.C., 2014. The Insight ToolKit image registration framework,. Front. Neuroinform. 8, 44.

Braak, H., Braak, E., 1991. Neuropathological stageing of Alzheimer-related changes. Acta Neuropathol. (Berl) 82, 239–259.

Braak, H., Braak, E., 1996. Evolution of the neuropathology of Alzheimer's disease. Acta Neurol. Scand. 94, 3–12.

Cho, H., Choi, J.Y., Hwang, M.S., Kim, Y.J., Lee, H.M., Lee, H.S., Lee, J.H., Ryu, Y.H., Lee, M.S., Lyoo, C.H., 2016a. In vivo cortical spreading pattern of tau and amyloid in the Alzheimer disease spectrum. Ann. Neurol. 80, 247–258.

Cho, H., Choi, J.Y., Hwang, M.S., Lee, J.H., Kim, Y.J., Lee, H.M., Lyoo, C.H., Ryu, Y.H., Lee, M.S., 2016b. Tau PET in Alzheimer disease and mild cognitive impairment. Neurology 87, 375–383.

Crary, J.F., Trojanowski, J.Q., Schneider, J.A., Abisambra, J.F., Abner, E.L., Alafuzoff, I., Arnold, S.E., Attems, J., Beach, T.G., Bigio, E.H., Cairns, N.J., Dickson, D.W., Gearing, M., Grinberg, L.T., Hof, P.R., Hyman, B.T., Jellinger, K., Jicha, G.A., Kovacs, G.G., Knopman, D.S., Kofler, J., Kukull, W.A., Mackenzie, I.R., Masliah, E., McKee, A., Montine, T.J., Murray, M.E., Neltner, J.H., Santa-Maria, I., Seeley, W.W., Serrano-Pozo, A., Shelanski, M.L., Stein, T., Takao, M., Thal, D.R., Toledo, J.B., Troncoso, J.C., Vonsattel, J.P., White, C.L., Wisniewski, T., Woltjer, R.L., Yamada, M., Nelson, P.T., 2014. Primary age-related tauopathy (PART): a common pathology associated with human aging. Acta Neuropathologica 128, 755–766.

Das, S.R., Avants, B.B., Grossman, M., Gee, J.C., 2009. Registration based cortical thickness measurement. Neuroimage 45, 867–879.

Das, S.R., Pluta, J., Mancuso, L., Kliot, D., Yushkevich, P.A., Wolk, D.A., 2015. Anterior and posterior MTL networks in aging and MCI. Neurobiol. Aging 36 Suppl 1. S141–S150, S150.e1.

Diehl, J.M., Arbinger, R., 1992. Einführung in die inferenzstatistik [Introduction to statistical inference], second ed. Eschborn bei Frankfurt am Main, Klotz.

Dronse, J., Fliessbach, K., Bischof, G.N., von Reutern, B., Faber, J., Hammes, J., Kuhnert, G., Neumaier, B., Onur, O.A., Kukolja, J., van Eimeren, T., Jessen, F., Fink, G.R., Klockgether, T., Drzezga, A., 2017. In vivo patterns of tau pathology, amyloid-β burden, and neuronal dysfunction in clinical variants of Alzheimer's disease. J. Alzheimer's Dis. 55, 465–471.

Frost, B., Jacks, R.L., Diamond, M.I., 2009. Propagation of tau misfolding from the outside to the inside of a cell. J. Biol. Chem. 284, 12845–12852.

Golla, S.S.V., Timmers, T., Ossenkoppele, R., Groot, C., Verfaillie, S., Scheltens, P., van der Flier, W.M., Schwarte, L., Mintun, M.A., Devous, M., Schuit, R.C., Windhorst, A.D., Lammertsma, A.A., Boellaard, R., van Berckel, B.N.M., Yaqub, M., 2017. Quantification of tau load using [(18)F]AV1451 PET. Mol. Imaging Biol. 19, 963–971.

Hyman, B.T., Trojanowski, J.Q., 1997. Editorial on consensus recommendations for the postmortem diagnosis of Alzheimer disease from the National Institute on Aging and the Reagan Institute Working Group on diagnostic criteria for the neuropathological assessment of Alzheimer disease. J. Neuropathol. Exp. Neurol. 56, 1095–1097.

Iaccarino, L., Tammewar, G., Ayakta, N., Baker, S.L., Bejanin, A., Boxer, A.L., Gorno-Tempini, M.L., Janabi, M., Kramer, J.H., Lazaris, A., Lockhart, S.N., Miller, B.L., Miller, Z.A., O'Neil, J.P., Ossenkoppele, R., Rosen, H.J., Schonhaut, D.R., Jagust, W.J., Rabinovici, G.D., 2018. Local and distant relationships between amyloid, tau and neurodegeneration in Alzheimer's Disease. Neuroimage. Clin. 17, 452–464.

Johnson, K.A., Schultz, A., Betensky, R.A., Becker, J.A., Sepulcre, J., Rentz, D., Mormino, E., Chhatwal, J., Amariglio, R., Papp, K., Marshall, G., Albers, M., Mauro, S., Pepin, L., Alverio, J., Judge, K., Philiossaint, M., Shoup, T., Yokell, D., Dickerson, B., Gomez-Isla, T., Hyman, B., Vasdev, N., Sperling, R., 2016. Tau positron emission tomographic imaging in aging and early Alzheimer disease. Ann. Neurol. 79, 110–119.

Josephs, K.A., Murray, M.E., Tosakulwong, N., Whitwell, J.L., Knopman, D.S., Machulda, M.M., Weigand, S.D., Boeve, B.F., Kantarci, K., Petrucelli, L., Lowe, V.J., Jack, C.R., Petersen, R.C., Parisi, J.E., Dickson, D.W., 2017. Tau aggregation influences cognition and hippocampal atrophy in the absence of beta-amyloid: a clinico-imaging-pathological study of primary age-related tauopathy (PART). Acta Neuropathologica 133, 705–715.

Klein, A., Tourville, J., 2012. 101 labeled brain images and a consistent human cortical labeling protocol. Front. Neurosci. 6, 171.

Klein, A., Andersson, J., Ardekani, B.A., Ashburner, J., Avants, B., Chiang, M.C., Christensen, G.E., Collins, L., Hellier, P., Song, J.H., Jenkinson, M., Lepage, C., Rueckert, D., Thompson, P., Vercauteren, T., Woods, R.P., Mann, J.J., Parsey, R.V., 2009. Evaluation of 14 nonlinear deformation algorithms applied to human brain MRI registration. NeuroImage 46, 786–802.

Landau, S.M., Breault, C., Joshi, A.D., Pontecorvo, M., Mathis, C.A., Jagust, W.J., Mintun, M.A. Alzheimer's Disease Neuroimaging Initiative, 2013. Amyloid-β imaging with Pittsburgh compound B and florbetapir: comparing radiotracers and quantification methods, Journal of nuclear medicine : official publication. Soc. Nucl. Med. 54, 70–77.

Landman, B., Warfield, S., 2012. Medical Image Computing and Computer Assisted Intervention Conference. MICCAI 2012 workshop on multi-atlas labeling.

LaPoint, M.R., Chhatwal, J.P., Sepulcre, J., Johnson, K.A., Sperling, R.A., Schultz, A.P., 2017. The association between tau PET and retrospective cortical thinning in clinically normal elderly. NeuroImage 157, 612–622.

Lewis, J., Dickson, D.W., 2016. Propagation of tau pathology: hypotheses, discoveries, and yet unresolved questions from experimental and human brain studies. Acta Neuropathologica 131, 27–48.

Lockhart, S.N., Schöll, M., Baker, S.L., Ayakta, N., Swinnerton, K.N., Bell, R.K., Mellinger, T.J., Shah, V.D., O'Neil, J.P., Janabi, M., Jagust, W.J., 2017. Amyloid and tau PET demonstrate region-specific associations in normal older people. NeuroImage 150, 191–199.

Lowe, V.J., Curran, G., Fang, P., Liesinger, A.M., Josephs, K.A., Parisi, J.E., Kantarci, K., Boeve, B.F., Pandey, M.K., Bruinsma, T., Knopman, D.S., Jones, D.T., Petrucelli, L., Cook, C.N., Graff-Radford, N.R., Dickson, D.W., Petersen, R.C., Jack, C.R., Murray, M.E., 2016. An autoradiographic evaluation of AV-1451 Tau PET in dementia. Acta Neuropathol. Commun. 4, 58.

Maass, A., Landau, S., Baker, S.L., Horng, A., Lockhart, S.N., Joie, R.L., Rabinovici, G.D., Jagust, W.J. Alzheimer's Disease Neuroimaging Initiative, 2017. Comparison of multiple tau-PET measures as biomarkers in aging and Alzheimer's Disease. NeuroImage 157, 448–463.

Marquié, M., Normandin, M.D., Vanderburg, C.R., Costantino, I.M., Bien, E.A., Rycyna, L.G., Klunk, W.E., Mathis, C.A., Ikonomovic, M.D., Debnath, M.L., Vasdev, N., Dickerson, B.C., Gomperts, S.N., Growdon, J.H., Johnson, K.A., Frosch, M.P., Hyman, B.T., Gómez-Isla, T., 2015. Validating novel tau positron emission tomography tracer [F-18]-AV-1451 (T807) on postmortem brain tissue. Ann. Neurol. 78, 787–800.

Mormino, E.C., Papp, K.V., Rentz, D.M., Schultz, A.P., LaPoint, M., Amariglio, R., Hanseeuw, B., Marshall, G.A., Hedden, T., Johnson, K.A., Sperling, R.A., 2016. Heterogeneity in suspected non-Alzheimer disease pathophysiology among clinically normal older individuals. JAMA Neurol. 73, 1185–1191.

Ossenkoppele, R., Schonhaut, D.R., Schöll, M., Lockhart, S.N., Ayakta, N., Baker, S.L., O'Neil, J.P., Janabi, M., Lazaris, A., Cantwell, A., Vogel, J., Santos, M., Miller, Z.A., Bettcher, B.M., Vossel, K.A., Kramer, J.H., Gorno-Tempini, M.L., Miller, B.L., Jagust, W.J., Rabinovici, G.D., 2016. Tau PET patterns mirror clinical and neuroanatomical variability in Alzheimer's disease. Brain 139 (Pt 5), 1551–1567.

Pontecorvo, M.J., Devous, M.D., Navitsky, M., Lu, M., Salloway, S., Schaerf, F.W., Jennings, D., Arora, A.K., McGeehan, A., Lim, N.C., Xiong, H., Joshi, A.D., Siderowf, A., Mintun, M.A. 18F-AV-1451-A05 investigators, 2017. Relationships between flortaucipir PET tau binding and amyloid burden, clinical diagnosis, age and cognition. Brain 140, 748–763.

Rafii, M.S., Lukic, A.S., Andrews, R.D., Brewer, J., Rissman, R.A., Strother, S.C., Wernick, M.N., Pennington, C., Mobley, W.C., Ness, S., Matthews, D.C. Down Syndrome Biomarker Initiative and the Alzheimer's Disease Neuroimaging Initiative, 2017. PET imaging of tau pathology and relationship to amyloid, longitudinal MRI, and cognitive change in Down syndrome: results from the Down Syndrome Biomarker Initiative (DSBI). J. Alzheimer's Dis. 60, 439–450.

Saint-Aubert, L., Lemoine, L., Chiotis, K., Leuzy, A., Rodriguez-Vieitez, E., Nordberg, A., 2017. Tau PET imaging: present and future directions. Mol. Neurodegener. 12, 19.

Schöll, M., Lockhart, S.N., Schonhaut, D.R., O'Neil, J.P., Janabi, M., Ossenkoppele, R., Baker, S.L., Vogel, J.W., Faria, J., Schwimmer, H.D., Rabinovici, G.D., Jagust, W.J., 2016. PET imaging of tau deposition in the aging human brain. Neuron 89, 971–982.

Schwarz, A.J., Yu, P., Miller, B.B., Shcherbinin, S., Dickson, J., Navitsky, M., Joshi, A.D., Devous, M.D., Mintun, M.S., 2016. Regional profiles of the candidate tau PET ligand 18F-AV-1451 recapitulate key features of Braak histopathological stages. Brain 139 (Pt 5), 1539–1550.

Sepulcre, J., Schultz, A.P., Sabuncu, M., Gomez-Isla, T., Chhatwal, J., Becker, A., Sperling, R., Johnson, K.A., 2016. In vivo tau, amyloid, and gray matter profiles in the aging brain. J. Neurosci. 36, 7364–7374.

Smith, S.M., Nichols, T.E., 2009. Threshold-free cluster enhancement: addressing problems of smoothing, threshold dependence and localisation in cluster inference. NeuroImage 44, 83–98.

Tosun, D., Landau, S., Aisen, P.S., Petersen, R.C., Mintun, M., Jagust, W., Weiner, M.W. Alzheimer's Disease Neuroimaging Initiative, 2017. Association between tau deposition and antecedent amyloid-β accumulation rates in normal and early symptomatic individuals. Brain 140, 1499–1512.

Tustison, N., Holbrook, N., Roberts, J., Avants, B., Cook, P., Stone, J., Gillen, D., Yassa, M., 2017. The ANTs Longitudinal Cortical Thickness Pipeline. The proceedings of The 13th International Conference on Alzheimer's & Parkinson's Diseases, Vienna, Austria.

Tustison, N.J., Cook, P.A., Klein, A., Song, G., Das, S.R., Duda, J.T., Kandel, B.M., van Strien, N., Stone, J.R., Gee, J.C., Avants, B.B., 2014. Large-scale evaluation of ANTs and FreeSurfer cortical thickness measurements. NeuroImage 99, 166–179.

Vemuri, P., Lowe, V.J., Knopman, D.S., Senjem, M.L., Kemp, B.J., Schwarz, C.G., Przybelski, S.A., Machulda, M.M., Petersen, R.C., Jack, C.R., 2017. Tau-PET uptake: regional variation in average SUVR and impact of amyloid deposition. Alzheimer's Dement. (Amsterdam, Netherlands) 6, 21–30.

Wang, H., Suh, J.W., Das, S.R., Pluta, J.B., Craige, C., Yushkevich, P.A., 2013. Multi-atlas segmentation with joint label fusion. IEEE Trans. Pattern Anal. Mach. Intell. 35, 611–623.

Wang, L., Benzinger, T.L., Su, Y., Christensen, J., Friedrichsen, K., Aldea, P., McConathy, J., Cairns, N.J., Fagan, A.M., Morris, J.C., Ances, B.M., 2016. Evaluation of tau imaging in staging Alzheimer disease and revealing interactions between β-amyloid and tauopathy. JAMA Neurol. 73, 1070–1077.

Whitwell, J.L., Dickson, D.W., Murray, M.E., Weigand, S.D., Tosakulwong, N., Senjem, M.L., Knopman, D.S., Boeve, B.F., Parisi, J.E., Petersen, R.C., Jack, C.R., Josephs, K.A., 2012. Neuroimaging correlates of pathologically defined subtypes of Alzheimer's disease: a case-control study. Lancet Neurol. 11, 868–877.

Whitwell, J.L., Josephs, K.A., Murray, M.E., Kantarci, K., Przybelski, S.A., Weigand, S.D., Vemuri, P., Senjem, M.L., Parisi, J.E., Knopman, D.S., Boeve, B.F., Petersen, R.C., Dickson, D.W., Jack, C.R., 2008. MRI correlates of neurofibrillary tangle pathology at autopsy: a voxel-based morphometry study. Neurology 71, 743–749.

Xia, C., Makaretz, S.J., Caso, C., McGinnis, S., Gomperts, S.N., Sepulcre, J., Gomez-Isla, T., Hyman, B.T., Schultz, A., Vasdev, N., Johnson, K.A., Dickerson, B.C., 2017. Association of in vivo [18F]AV-1451 tau PET imaging results with cortical atrophy and symptoms in typical and atypical Alzheimer disease. JAMA Neurol. 74, 427–436.

Xie, L., Wisse, L.E., Das, S.R., Wang, H., Wolk, D.A., Manjón, J.V., Yushkevich, P.A., 2016. Accounting for the Confound of Meninges in Segmenting Entorhinal and Perirhinal Cortices in T1-weighted MRI. International Conference on Medical Image Computing and Computer-Assisted Intervention, pp. 564–571.

Yekutieli, D., Benjamini, Y., 1999. Resampling-based false discovery rate controlling multiple test procedures for correlated test statistics. J. Stat. Plann. Inference 82, 171–196.

Yushkevich, P.A., Pluta, J.B., Wang, H.Z., Xie, L., Ding, S.L., Gertje, E.C., Mancuso, L., Kliot, D., Das, S.R., Wolk, D.A., 2015. Automated volumetry and regional thickness analysis of hippocampal subfields and medial temporal cortical structures in mild cognitive impairment. Hum. Brain Mapp. 36, 258–287.